JACS
ARTICLES

Size-Dependent Spontaneous Alloying of Au−Ag Nanoparticles

Tomohiro Shibata,[†] Bruce A. Bunker,[*,†] Zhenyuan Zhang,[‡,§] Dan Meisel,[*,‡,§]
Charles F. Vardeman II,[‡,§] and J. Daniel Gezelter[*,‡]

Contribution from the Department of Physics, Department of Chemistry and Biochemistry, and The Notre Dame Radiation Laboratory, University of Notre Dame, Notre Dame, Indiana 46556

Received May 2, 2002

Abstract: We report on systematic studies of size-dependent alloy formation of silver-coated gold nanoparticles (NPs) in aqueous solution at ambient temperature using X-ray absorption fine structure spectroscopy (XAFS). Various Au-core sizes (2.5−20 nm diameter) and Ag shell thicknesses were synthesized using radiolytic wet techniques. The equilibrium structures (alloy versus core−shell) of these NPs were determined in the suspensions. We observed remarkable size dependence in the room temperature interdiffusion of the two metals. The interdiffusion is limited to the subinterface layers of the bimetallic NPs and depends on both the core size and the total particle size. For the very small particles (≤4.6 nm initial Au-core size), the two metals are nearly randomly distributed within the particle. However, even for these small Au-core NPs, the interdiffusion occurs primarily in the vicinity of the original interface. Features from the Ag shells do remain. For the larger particles, the boundary is maintained to within one monolayer. These results cannot be explained either by enhanced self-diffusion that results from depression of the melting point with size or by surface melting of the NPs. We propose that defects, such as vacancies, at the bimetallic interface enhance the radial migration (as well as displacement around the interface) of one metal into the other. Molecular dynamics calculations correctly predict the activation energy for diffusion of the metals in the absence of vacancies and show an enormous dependence of the rate of mixing on defect levels. They also suggest that a few percent of the interfacial lattice sites need to be vacant to explain the observed mixing.

Introduction

It is now well established that small particles in the nanometer size regime exhibit physical and chemical properties that differ markedly from those of the bulk material. The enormous surface area-to-mass ratio of nanoparticles (NPs) leads to excess surface free energy that is comparable to the lattice energy, leading in turn to structural instabilities. A common example is the depression of the melting temperature (T_{m}) or melting pressure in metallic and semiconductor NPs.[1−9] These size effects may appear in binary metal NPs as size-dependent alloy formation.[10−15] Mori and co-workers reported spontaneous alloying of Cu,[10,12,13] Zn,[11] Pb,[16] and Sb[14] into gold, at ambient or even subambient temperatures.[12] These studies utilized transmission electron microscopy (TEM) and diffraction methods to determine the change in lattice parameters that results from the alloying process. In this report, we focus on Au−Ag NPs, prepared initially as core−shell structures in aqueous suspensions at ambient temperature. The lattice parameters of alloys of these two metals, Au and Ag, remain essentially unchanged at any atomic ratio.

The mechanism for alloying of small particles is still not clear. Kinetic considerations indicate that, for the two metals to mix, the diffusion coefficient needs to be many orders of magnitude larger than that for the bulk materials.[11,12] Shimizu et al. reproduced Mori and Yasuda's results of rapid alloying using two-dimensional molecular dynamics simulation and concluded that the surface melting plays an important role.[17] However, they used relatively small NPs (∼100 atoms). Recent studies on Sn alloying at Cu surfaces reveal a process driven by surface

---

[*] To whom correspondence should be addressed. E-mail: (B.A.B.) bunker.1@nd.edu, (D.M.) dani@nd.edu, (J.D.G.) gezelter@nd.edu.

[†] Department of Physics.

[‡] Department of Chemistry and Biochemistry.

[§] The Notre Dame Radiation Laboratory.

(1) Pawlow, P. *Z. Phys. Chem.* **1909**, *65*, 545.
(2) Buffat, P.; Borel, J.-P. *Phys. Rev. A* **1976**, *13*, 2287.
(3) Solliard, C.; Flueli, M. *Surf. Sci.* **1985**, *156*, 487.
(4) Goldstein, A. N.; Echer, C. M.; Alivisatos, A. P. *Science* **1992**, *256*, 1425.
(5) Haase, M.; Alivisatos, A. P. *J. Phys. Chem.* **1992**, *96*, 6756.
(6) Tolbert, S. H.; Alivisatos, A. P. *Z. Phys. D* **1993**, *26*, 56.
(7) Tolbert, S. H.; Herhold, A. B.; Brus, L. E.; Alivisatos, A. P. *Phys. Rev. Lett.* **1996**, *76*, 4384.
(8) Herhold, A. B.; Tolbert, S. H.; Guzelian, A. A.; Alivisatos, A. P. In *Fine Particles Science and Technology. From Micro to Nano Particles*; Pelizzetti, E., Ed.; Kluver Academic, NATO ASI Series: Dordrecht, 1996; Vol. 3/12, p 331.
(9) Chen, C.-C.; Herhold, A. B.; Johnson, C. S.; Alivisatos, A. P. *Science* **1997**, *276*, 398.
(10) Mori, H.; Komatsu, M.; Takeda, K.; Fujita, H. *Philos. Mag. Lett.* **1991**, *63*, 173.
(11) Yasuda, H.; Mori, H. *Phys. Rev. Lett.* **1992**, *69*, 3747.
(12) Yasuda, H.; Mori, H.; Komatsu, M.; Takeda, K. *J. Appl. Phys.* **1993**, *73*, 1100.
(13) Mori, H.; Yasuda, H.; Kamino, T. *Philos. Mag. Lett.* **1994**, *69*, 279.
(14) Mori, H.; Yasuda, H. *Mater. Sci. Eng., A* **1996**, *217/218*, 244.
(15) Yasuda, H.; Mori, H. *Ann. Phys.* **1997**, *22*, C2.
(16) Yasuda, H.; Mori, H. *Philos. Mag.* **1996**, *A73*, 567.
(17) Shimizu, Y.; Ikeda, K.; Sawada, S. *Phys. Rev. B* **2001**, *64*, 075412.

10.1021/ja026764r CCC: $22.00 © 2002 American Chemical Society

free energy that leads to migration of tin atoms at the NPs surface.[18] Because T_m of the smaller particles is much lower than the corresponding bulk, much faster interdiffusion of the atoms is expected in NPs. Preservation of twinning boundaries during the alloying of copper in gold NPs led Mori et al. to conclude that the particles remain solid during the alloying process.[13] Nonetheless, because the diffusion coefficient at the melting point is essentially independent of the size, the diffusion in the solid particles is expected to be faster in the smaller particles at similar temperatures.[19] Whether the alloying process can be understood by surface diffusion alone or it requires additional effects, such as morphological changes or defect creation at the interface, remains to be answered. A number of studies on mechanical alloying have suggested that interfacial imperfections enhance the diffusion by many orders of magnitude.[20] It is also clear that often-used supports play an important role in the crystallization and morphology of NPs.[21] Most of the previous structural studies were carried out on NPs deposited on solid supports. We therefore chose to study the structure of NPs in the absence of a solid support to approach their intrinsic properties. However, the NPs in our study maintain a layer of stabilizer molecules, which is necessary to prevent coagulation.

X-ray absorption fine structure spectroscopy (XAFS) has proven useful in identifying random or preferred occupation of the sites around specific atoms. Using XAFS, interatomic distances, and variation in the distances (i.e., Debye Waller factors (DWF)), the identity and number of nearest neighboring atoms (coordination numbers, labeled below CN) within the first few coordination shells of the X-ray excited atoms can be determined. The structural information is averaged over all of the X-ray excited atoms in the entire samples, but due to the fact that a large percentage of the atoms in the NPs is at the interface, the information obtained is sensitive to the bimetallic interfacial structure. Using XAFS, we studied NPs of silver deposited on gold core (Au−Ag hereafter) suspended in aqueous solution. One reason to choose the Au−Ag systems is the similarity between Au and Ag, particularly their similar atomic sizes. Complete miscibility of that pair of metals can be obtained in the bulk at any composition with no change in lattice parameters, and the bulk random alloys are free of local strains.[22] Therefore, our Au−Ag NPs, prepared initially as core−shell structures, are particularly suitable for studying the fundamental mechanism of atomic migration in the NPs. Combinations of Au and Ag have been extensively studied, often because of the great interest in their plasmon band.[23,24] In characterizing Au−Ag particles using TEM, Hodak et al. have shown clear phase boundaries between the Au core and the Ag shell for particle sizes ≥20 nm.[25] For particles of smaller sizes, the phase boundaries are not observed. Our results concur with a sharp phase boundary in the larger particles, but we show that as the size decreases the two metals intermix. Recent reports using laser-induced melting of mono- and bimetallic nanoparticles outlined the events that lead to melting and intermetallic mixing of the two metals.[25−28] Furthermore, light-induced melting has recently been used to control the shape and morphology of metallic NPs and thereby manipulate their absorption characteristics.[29] On the other hand, the depression of T_m in NPs was used to thermally control their shape.[30,31] Here we report on the size-dependent spontaneous alloying of Ag into Au small particles suspended in solution.

Experimental Section

A. Synthesis. The NPs were prepared using the radiolytic methodology developed by Henglein and co-workers to reduce Au(III), Au(I), or Ag(I) ions to their metallic state.[25,32−36] The Au-core particles were prepared in a two-step procedure. First, the smallest core particles (2.5 nm) were synthesized, and then these seed particles were enlarged to provide the variable Au-core sizes onto which Ag was subsequently deposited. The advantage of this approach, rather than preparing the desired core size in a one-step synthesis, is the narrowing of the size distribution of the final particles.[34] The procedure to obtain the core−shell NPs follows:

1. Synthesis of Gold-Seed Particles. Briefly, for 2.5 nm particles, aqueous solutions containing $(4-6) \times 10^{-4}$ M $NaAuCl_4$, 0.5 M methanol, and 10^{-2} M poly-vinyl alcohol (PVA, M_w 50 000−85 000) were deaerated by bubbling Ar, and then irradiated in a ^{60}Co-γ source at a dose rate of 1.5×10^3 krad/h. The radiation period depended on $[AuCl_4^-]$ and varied from 16 to 24 min. This corresponds to approximately twice the dose required for total reduction of Au(III) assuming a yield of 6 reduction equivalents per 100 eV of irradiation. The orange-brown sol is very sensitive to air; therefore, all manipulations of all suspensions were carried out in airtight vessels in a glovebox under Ar. Au-core particles larger than 15 nm were prepared using the Turkevich citrate method.[37]

2. Enlargement of the Core. The concentration of additional Au needed to obtain a desired size was estimated using eq 1:

$$d_1 = (C_1/C_0)^{1/3} d_0 \tag{1}$$

where C and d are total Au concentration and particle diameter, respectively, and the subscripts 0 and 1 refer to the first and second preparations, respectively. Seed particles from the previous step (to give C_0) were mixed with the corresponding volume of a deaerated solution containing 0.5 M methanol, $1-2 \times 10^{-4}$ M sodium citrate (as a stabilizer/buffer but not a reductant), and the desired amount of $KAu(CN)_2$ (to give C_1). It has been shown that reduction of the cyano complex in this system occurs only at the surface of the preexisting seed particles.[34] The mixture was purged with ultrapure N_2O and then irradiated at a dose rate of 2.3×10^2 krad/h for larger than the theoretical dose needed to provide complete reduction of the Au(I) complex (assuming 6 molecule/100 eV of reducing equivalents), until no change was observed in the plasmon absorption band. Following the irradiation,

---

(18) Schmid, A. K.; Bartelt, N. C.; Hwang, R. Q. *Science (Washington, D.C.)* **2000**, *290*, 1561.

(19) Dick, K.; Dhanasekaran, T.; Zhang, Z.; Meisel, D. *J. Am. Chem. Soc.* **2002**, *124*, 2312.

(20) Das, D.; Chatterjee, P.; Manna, I.; Pabi, S. *Scr. Mater.* **1999**, *41*, 861.

(21) Fujimoto, T.; Kojima, I.; Onuma, K. *Nanostruct. Mater.* **1998**, *10*, 65.

(22) Frenkel, A. I.; Machavariani, V. S.; Rubshtein, A.; Rosenberg, Y.; Voronel, A.; Stern, E. A. *Phys. Rev. B* **2000**, *62*, 9364.

(23) Link, S.; El-Sayed, M. A. *J. Phys. Chem. B* **1999**, *103*, 8410.

(24) Link, S.; El-Sayed, M. A. *J. Phys. Chem. B* **1999**, *103*, 4212.

(25) Hodak, J. H.; Henglein, A.; Giersig, M.; Hartland, G. V. *J. Phys. Chem. B* **2000**, *104*, 11708.

(26) Fujiwara, H.; Yanagida, S.; Kamat, P. V. *J. Phys. Chem. B* **1999**, *103*, 2589.

(27) Link, S.; Wang, Z. L.; El-Sayed, M. A. *J. Phys. Chem. B* **1999**, *103*, 3529.

(28) Link, S.; Wang, Z. L.; El-Sayed, M. A. *J. Phys. Chem. B* **2000**, *104*, 7867.

(29) Jin, R.; Cao, Y.; Mirkin, C. A.; Kelly, K. L.; Schatz, G. C.; Zheng, J. G. *Science* **2001**, *294*, 1901.

(30) Maye, M. M.; Zheng, W.; Leibowitz, F. L.; Ly, N. K.; Zhong, C. J. *Langmuir* **2000**, *16*, 490.

(31) Maye, M. M.; Zhong, C.-J. *J. Mater. Chem.* **2000**, *10*, 1895.

(32) Mulvaney, P.; Giersig, M.; Henglein, A. *J. Phys. Chem.* **1993**, *97*, 7061.

(33) Henglein, A. *Langmuir* **1999**, *15*, 6738.

(34) Henglein, A.; Meisel, D. *Langmuir* **1998**, *14*, 7392.

(35) Hodak, J. H.; Henglein, A.; Hartland, G. V. *J. Phys. Chem. B* **2000**, *104*, 5053.

(36) Treguer, M.; Cointet, C.; Remita, H.; Khatouri, J.; Mostafavi, M.; Amblard, J.; Belloni, J.; Keyzer, R. *J. Phys. Chem. B* **1998**, *102*, 4310.

(37) Turkevich, J.; Stevenson, P. C.; Hillier, J. *Discuss. Faraday Soc.* **1951**, *11*, 55.

Table 1. Samples Used in the Present Study; Au-Core Diameter with Various Ag Atomic Layers (1 AL = 2.36 Å)[a]

sample	[Ag]/[Au]	initial Au-core size	Ag layers (assuming core–shell)	total size
A	0.44	2.5 nm	0.3 nm/1.1 AL	3.1 nm
B	0.8	2.5 nm	0.9 nm/3.8 AL	4.3 nm
C	0.91	2.5 nm	1.6 nm/6.5 AL	5.6 nm
D	0.33	3.5 nm	0.3 nm/1.1 AL	4.0 nm
E	0.33	4.6 nm	0.4 nm/1.4 AL	5.3 nm
F	0.67	4.6 nm	1.0 nm/4.3 AL	6.6 nm
G	0.83	4.6 nm	1.9 nm/7.9 AL	8.3 nm
H	0.23	8.3 nm	0.4 nm/1.4 AL	9.0 nm
I	0.44	8.3 nm	0.9 nm/3.8 AL	10.1 nm
J	0.75	8.3 nm	2.5 nm/10.4 AL	13.2 nm
K	0.11	20 nm	0.4 nm/1.7 AL	20.8 nm
L	0.2	20 nm	0.7 nm/3.1 AL	21.4 nm
M	0.33	20 nm	1.4 nm/6.4 AL	22.8 nm

[a] Sample labeling in Table 1 corresponds to the labeling in Figures 4 and 5.

Amberlite MB-150 ion-exchange resin was used to remove excess cyanide and citrate ions (all manipulations in a glovebox). The size of the particles in each enlargement batch was determined by TEM. Actual sizes were within ±20% of those calculated from eq 1.

3. Deposition of Silver Shell. Gold-core sols of the desired size were mixed with a deaerated solution containing 0.5 M methanol, $(1-2) \times 10^{-4}$ M sodium citrate, and the required concentration of $KAg(CN)_2$ in a glovebox under Ar. The concentration of the silver cyanide complex was varied to obtain the various thickness of Ag shell. The mixture was saturated with N_2O and irradiated at dose rates of $(0.67-2.3) \times 10^5$ rad/h. The sol was then treated with the same ion-exchange resin to remove any excess ions. Colors of the sols varied from red-brown to light yellow, depending on the amount of Ag deposited. Absorption spectra were taken during the reduction, and completion of the reduction was confirmed spectrophotometrically when no further change in the spectra could be noticed. It is now established,[25,35] and was verified here by TEM, that this procedure generates Au−Ag particles of core−shell structures for large particles (>15 nm). Table 1 summarizes the dimensions of the particles that were studied in this report. Up to approximately 10 atomic layers (AL), with one AL = 2.36 Å, assuming fcc (111) stacking, were studied.

The solid−electrolyte interface of the particles necessarily carries stabilizing species, mostly citrate or PVA in the preparations described above. However, no effect of the stabilizer at the interface on the XAFS spectra was observed. Optical absorption spectra were taken before and after the XAFS measurements with no indication of sol degradation.

B. Characterization. Mean particle diameters, particle size distribution, and morphology were determined by TEM. Typically, the size distribution decreases upon enlargement of the particles, for 2.5 nm ± 10% and 20 nm ± 5% were observed. It was verified for all preparations, by analysis of the plasmon band, that immediately after the deposition of Ag the NPs retained core−shell structures. The time dependence of the optical spectra strongly depends on the NPs size; for the 2.5 nm NPs, the equilibrium is reached in a few days (vide infra), while for larger particles, the spectra changed only little within a week.

All XAFS experiments were performed at the MRCAT beamline at the Advanced Photon Source of Argonne National Laboratory. Measurements were performed at the Au L_3 ($E_0 = 11\,918$ eV) and Ag K edges ($E_0 = 25\,514$ eV) with the samples at room temperature. Because of the low concentration of the metals in the samples, the measurements involved X-ray fluorescence detection with a thick X-ray filter and Soller slits to reduce scattered background.[38] Water radiolysis generates hydrogen bubbles, which can interfere with the measurements. Therefore, more than 10 fast XAFS scans were taken, each on a fresh sample, and the spectra were averaged. Both incident and fluorescence X-rays were detected by a gas-filled ionization chamber. The solutions were kept in a glass cell with an X-ray window filled with argon gas to maintain inert atmosphere. All measurements were performed within one week following the synthesis, and all of the NPs were verified to be in thermodynamic equilibrium (no spectral changes in the plasmon region).

The XAFS oscillations, $\chi(k)$ (where k is the photoelectron wavenumber), were extracted by standard procedures.[39] The Fourier transformed data were analyzed using the UW package.[40,41] Only nearest neighbors, including scattering from Au and Ag, were fit. However, for most of the NPs, higher neighbor peaks were discernible down to 2.5 nm, indicating that the particles are not highly disordered or liquid droplets. No evidence of scattering from the solvent was observed, presumably because of the large DWF. In the present systems, higher order cumulants are not negligible at room temperatures. Fortunately though, these usually affect bond lengths and are relatively insensitive to the coordination numbers as long as the DWF for the various pairs, Au−Au, Au−Ag, and Ag−Ag, have similar values. Indeed, analyses with and without the cumulants essentially do not change our results with regard to alloying. Because low temperature measurements are not possible for the NP in solution, we cannot determine the cumulants and the bond length changes. We thus limit the discussion only to the coordination analysis in this report.

For the Au−Ag NPs, the data from Au L_3 and Ag K edges were fit simultaneously using the common parameters of bond length, and the constraint of the coordination numbers (CNs), $N_{Au}^{Ag} = x/(1 - x)N_{Ag}^{Au}$, was used for $Au_{1-x}Ag_x$.[42] Here the parameter N_A^B is the CN of species B around atom A, and N_A^{tot} is the sum of the scattering from Au and Ag around atom A. The reduction in CN due to the increased specific surface area with reduction in size is expected to be small (<5%), within the uncertainty of CN (±10%). The simultaneous fits usually give smaller uncertainties, but separate fits at Au and Ag edges give essentially the same result. In all fits, CNs of X_{Au}^{Ag} ($\equiv N_{Au}^{Ag}/N_{Au}^{tot}$), N_{Au}^{tot}, and N_{Ag}^{tot}, the DWF, and the Au−Au, Au−Ag, and Ag−Ag bond lengths were fit as variable parameters. For some of the Au−Ag particles, only the Au L_3 edge provided useful results because of the lower concentration of Ag in those suspensions. Nonetheless, for those cases where data from Au L_3 and Ag K edges were both available, essentially the same results were obtained.

C. Molecular Dynamics Simulations. To gain insight into the alloying process, molecular dynamics simulations were conducted on model spherical particles composed of Ag and Au atoms interacting under the embedded atom method (EAM) potential[43,44] using Johnson's mixing rule[45] for the Ag−Au cross potentials. The choice of mixing rules is somewhat arbitrary, but the Johnson rule predicts heats of solution for many alloys that are consistent with experimental observations and is therefore commonly used in the literature. Because the lattice constants for Ag and Au are nearly identical, the particles were constructed in a perfect fcc lattice using the average of the two-lattice constants (4.085 Å). Those atoms inside the core radius (r_{core}) were initialized with Au parameters, while those between the core and shell radius ($r_{core} < r < r_{shell}$) were initialized as Ag atoms. A 2 Å thick shell centered on r_{core} was designated as the "interface" region, as shown in Figure 1. For calculations involving interfacial vacancies, 5% or 10% of these interfacial atoms were chosen at random and were removed from the initial configuration. For the simulations described

---

(38) Stern, E. A.; Heald, S. *Rev. Sci. Instrum.* **1979**, *50*, 1579.

(39) Koningsberger, D. C.; Prins, R. *X-ray Absorption: Principles, Applications, Techniques of EXAFS, SEXAFS, and XANES*; Wiley: New York, 1988.

(40) Rehr, J.; Albers, R.; Zabinski, S. *Phys. Rev. Lett.* **1992**, *69*, 3397.

(41) Newville, M.; Ravel, B.; Haskel, D.; Stern, E.; Yacoby, Y. *Physica B* **1995**, *208–209*, 154. Data were fit by FEFFIT using the theoretical paths produced by FEFF601.

(42) Frenkel, A. I.; Machavariani, S. V.; Rubshtein, A.; Rosenberg, Y.; Voronel, A.; Stern, E. A. *Phys. Rev. B* **2000**, *62*, 9364.

(43) Daw, M. S.; Baskes, M. I. *Phys. Rev. B* **1984**, *29*, 6443.

(44) Foiles, S. M.; Baskes, M. I.; Daw, M. S. *Phys. Rev. B* **1986**, *33*, 7983.

(45) Johnson, R. A. *Phys. Rev. B* **1989**, *39*, 12554.

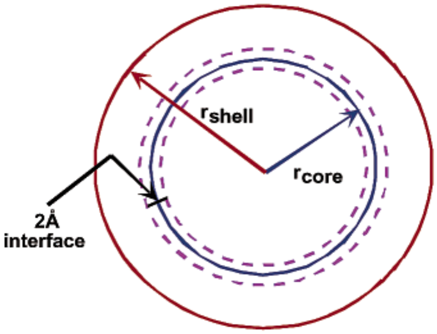

Figure 1. Diagram of the initial geometry of the NP simulations. Vacancies were created by removing atoms at random from the 2 Å shell surrounding the interface.

here, $r_{core} = 12.5$ Å and $r_{shell} = 19.98$ Å. These radii match the smallest of the NPs described in the Experimental Section above (B in Table 1). The total number of atoms in each nanoparticle was 1926 (no vacancies), 1914 (5% interfacial vacancies), and 1902 (10% interfacial vacancies).

Before starting the molecular dynamics runs, a relatively short steepest-descent minimization was performed to relax the lattice in the initial configuration. During the initial 30 ps of each trajectory, velocities were repeatedly sampled from a Maxwell–Boltzmann distribution matching the target temperature for the run. Following this initialization procedure, trajectories were run in the constant-NVE (number, volume, and total energy) ensemble with zero initial total angular momentum. To compare the structural features obtained from the NVE-ensemble molecular dynamics, additional trajectories were run using a modified Nosé–Hoover thermostat to maintain constant temperature (NVT) and zero total angular momentum. Data collection for all of the simulations started after the 30 ps equilibration period had been completed. We simulated particles with the above-mentioned interfacial vacancy density at 100 K intervals from 500 to 1200 K. Given the masses of the constituent atoms, we were able to use time steps of 5 fs while maintaining excellent energy conservation. Typical simulation times were 100 ns for nanoparticles simulated at 500–600 K and 12–24 ns for particles at 600–1200 K.

Results and Discussion

Rate of Alloying. The spectrum of 2.5 nm Au-core particles coated with 3 AL of Ag immediately following the preparation is shown in Figure 2. Also shown in this figure are the spectral changes of the particles during the first few days following the preparation. No change was observed in the spectrum after the third day, and the spectrum remained unchanged for another week. The initial spectrum indicates some alloying at early stages. The final one (day 3 after synthesis, Figure 2) resembles the spectrum of a random alloy.[36,46] Assuming that the evolution of spectra in Figure 2 represents the rate of alloying, one can estimate the diffusion coefficient, D, of Ag in Au using the proper diffusion equation: $D = (d_0/2)^2/6t$. This yields $D \approx 1.0 \times 10^{-20}$ cm^2 s^{-1}. Close examination of the final spectra in Figure 2 reveals the appearance of two absorption bands at 205 and 211 nm. These are assigned to $\mathrm{Au(CN)_2}^-$ on the basis of genuine spectra of the Au(I) cyanide complex. Oxidation at the surface occurs presumably by traces of oxygen. Thus, some Au migrated from the core to the surface of the particles during this time, in agreement with the proposed alloying process. Similar results were obtained for particles of 2.5 nm Au core with 5 AL. However, the time for equilibration was longer, 4 days, indicating that the rate of alloying depends on the total size of the particle and not merely the core. A similar conclusion is drawn below from the structural determinations.

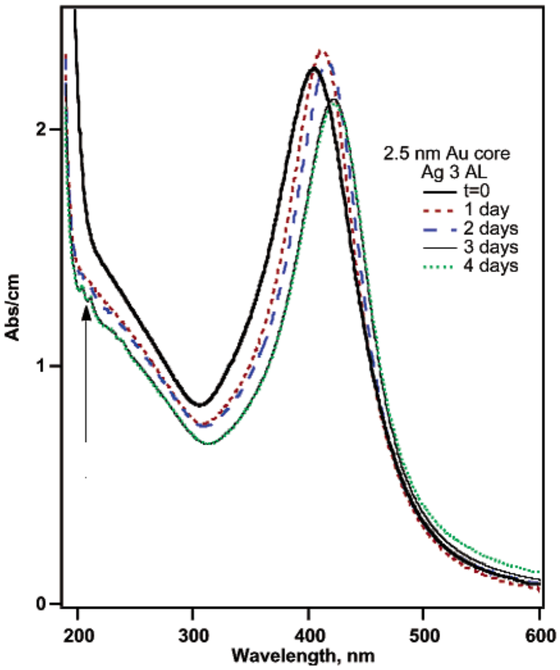

Figure 2. Spectral evolution of the plasmon band of 2.5 nm Au core coated with 3 AL of Ag. The absorption bands due to the Au-cyanide complex in the UV region are highlighted with an arrow.

Structures. Figure 3a shows the Au L_3 edge XAFS spectrum ($\chi(k)$) of the initial 2.5 nm Au-core NPs coated with 1.1, 3.8, and 6.5 ALs of Ag. Clearly, a phase shift in $\chi(k)$ is seen, and Au–Ag in the first shell appears as a doublet in the Fourier transform of $\chi(k)$ (Figure 3b). The doublet components, though, vary with the amount of deposited Ag. This indicates a significant amount of Ag in the nearest-neighbor shell around Au because the phase shift and the amplitude of the backscattering function between Au and Ag above 6 Å^{-1} are quite different. This large difference facilitates the coordination analysis of the Au–Ag system.

The fit parameter X_{Au}^{Ag} reflects the degree of alloy formation and is plotted in Figure 4 as a function of the total NP size (see also Table 1). NPs with different initial Au-core size are identified in Figure 4 by different symbols. In a completely random alloy, X_{Au}^{Ag} would follow the dashed lines upon Ag deposition; for phase segregated NPs, X_{Au}^{Ag} would be a small number, independent of Ag deposition (once the first AL is formed), as shown at the bottom of the figure (dot-dash lines). Both extreme cases were calculated from the size of the NPs assuming fcc structure and (111) face at the interfaces.

Alloy structures were simulated to visualize possible interdiffused structures. Starting with phase segregated structures, the interdiffusion of Au and Ag atoms was modeled by randomly exchanging nearest neighbors. The exchange probability for Au and Ag atoms was assumed to be the same because the diffusion coefficients of each metal in itself, or in the other metal, are identical. The simulation was terminated when near-neighbor statistics were consistent with the CNs in Figure 4. The resulting cross sections (fcc (111) face) for several structures identical to the CN obtained experimentally are shown in Figure 5, where Au and Ag are depicted as black and white circles, respectively.

---

(46) Link, S.; Wang, Z. L.; El-Sayed, M. A. *J. Phys. Chem. B* **1999**, *103*, 3529.

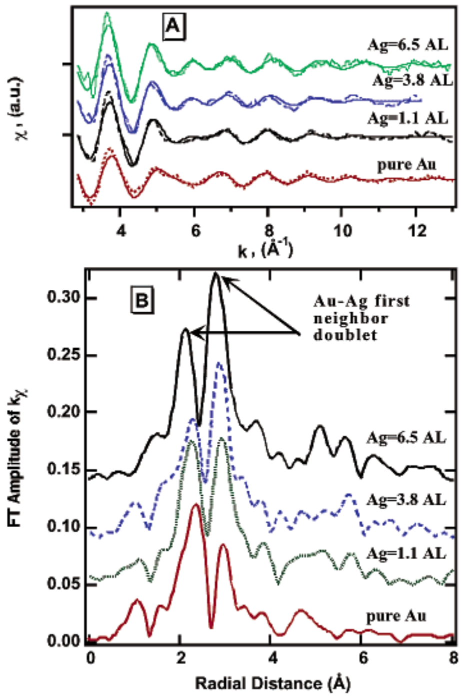

Figure 3. (a) Au L_3 edge XAFS oscillations, $\chi(k)$, for 2.5 nm pure Au particles, and Au initially coated with 1.1, 3.8, and 6.5 AL of Ag. They correspond to (A), (B), and (C), respectively, in Table 1. Experimental spectra (dotted lines) are shifted along the *y*-axis for clarity. The fits for the Au/Ag first neighbors are also shown (solid lines). Note the change of the oscillatory features above approximately $k = 6$ Å^{-1} with the increase of the Ag deposition. This results from the increase of the Ag near neighbors around Au atoms, because Au and Ag have quite different backscattering phase shifts at higher *k*. (b) Magnitude of the Fourier transform of $k\chi(k)$ for the same samples, where $k = 3-11$ Å^{-1} is transformed. Spectra are shifted vertically for clarity. The change in $\chi(k)$ in Figure 3a appears clearly as the change of the intensity ratio of the doublet features highlighted by the arrows. The peak intensity at larger distance increases relative to that of the peak at smaller distance with increasing Ag deposition due to changes in interference between the Au and Ag oscillations. Note that both peaks come from the first neighbor (with a single distance), and they appear at a shorter distance from the actual bond lengths because of the backscattering phase shift.

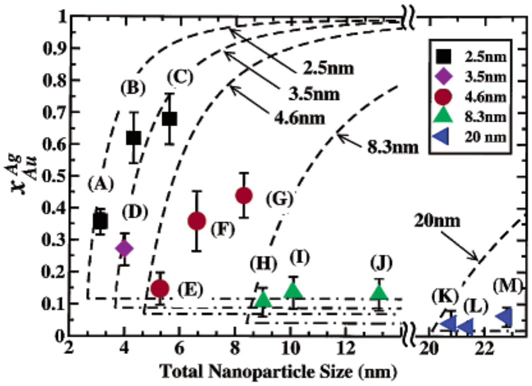

Figure 4. The fraction of Ag near neighbors around Au, $X_{\mathrm{Au}}^{\mathrm{Ag}}$, as a function of total NPs size for various initial Au-core sizes and with various Ag thickness. Different initial Au-core sizes are depicted as different symbols. Dashed curves indicate a random alloy for the corresponding initial core size. Dot-dash straight lines indicated phase segregated core−shell structures. Capital letters refer to the compositions in Table 1.

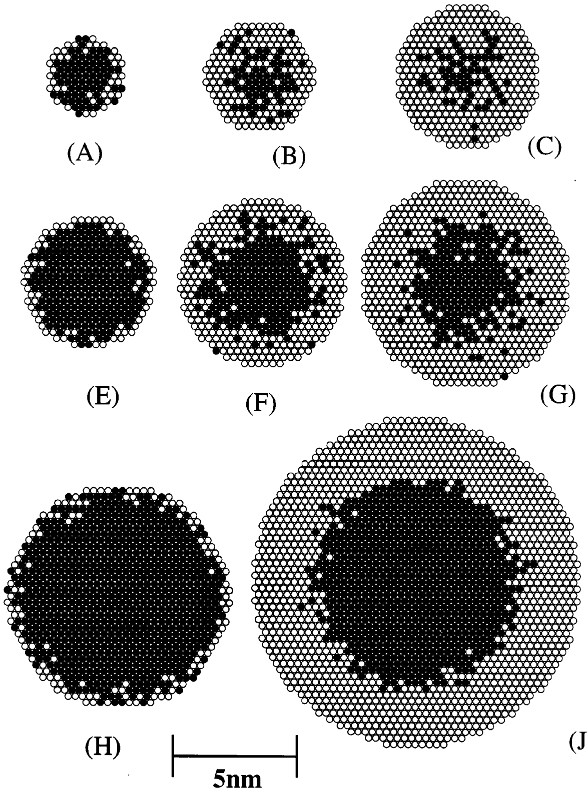

Figure 5. Simulated alloy structures consistent with the observed CNs in Figure 4. The fcc(111) face passing through the center is shown for several NPs. Au and Ag atoms are depicted as black and white circles, respectively. Capital letters refer to the composition in Table 1.

As can be seen in Figure 4, increasing the Ag shell thickness hardly affects the fraction $X_{\mathrm{Au}}^{\mathrm{Ag}}$ for NPs of Au-initial core size >8.3 nm (e.g., points H, I, J or K, L, M). A few percent of the near neighbors to gold are silver, and this percentage is independent of shell thickness. This indicates a distinct interface with little interdiffusion at the bimetallic interface. Such a structure is shown, for example, in Figure 5H and J. On the other hand, for ≤4.6 nm initial Au core, $X_{\mathrm{Au}}^{\mathrm{Ag}}$ shows strong dependence on shell thickness. It increases upon increasing the thickness from one to four ALs (e.g., Figure 4E−G), indicating that the interdiffusion lengths increase near the interface and the alloying extends to nearly 10 ALs. However, it is also clear from Figure 4 that as the thickness increases, $X_{\mathrm{Au}}^{\mathrm{Ag}}$ increasingly deviates from the random alloy curve (e.g., compare Figure 4 points A and C or F and G). The structures of Figure 5F and G show that the alloying is in the vicinity of the *buried* interface. This thickness dependence is similar for the 2.5 nm initial Au-core NPs. However, in the latter the initial Au core is almost completely randomized as shown in Figure 5B and C. It should be emphasized that all of these NPs have distinct core−shell structures at the time of the synthesis. Therefore, two questions may arise: (i) What is the mechanism of the size-dependent rate of alloying? (ii) Why does the alloying stop beyond the *buried* interface rather than proceed to a complete random alloy?

Size-dependent alloying can, in principle, result from an increase in the diffusion coefficient of the metals, which in turn is related to the depression of melting point of the particles as their size decreases.[2] A recent report attempts to make this correlation to conclude that the diffusion coefficient of gold in gold NPs of 2 nm is approximately $D = 1 \times 10^{-24}$ cm^2 s^{-1} at room temperature.[19] Whereas this value is much larger than the bulk value of $D = 1 \times 10^{-32}$ cm^2 s^{-1}, it is too small to rationalize the present observations. As shown above, and because the structural measurements were made within a week from synthesis, a diffusion coefficient of the order of $D = 1 \times 10^{-20}$–1×10^{-21} cm^2 s^{-1} is necessary. Moreover, if excess surface free energy were the major effect for the observed alloying, complete randomization would be expected. The remaining shell structure between the interface and the outer surface should randomize as well. Surface melting is also excluded as a mechanism for the alloying because crystalline features were observed in the XAFS spectra resulting from higher neighbors in pure Au NPs down to 2.5 nm particles. In these particles, approximately 40% of the atoms reside at the surface. Thus, excess surface free energy cannot in itself rationalize the observations.

To explain the faster-than-expected diffusion, and to rationalize preferential randomization at the subsurface layers but not deeper, we invoke a relatively high density of defects, particularly vacancies, at the bimetallic interface. Such defects may be caused by the surface curvature or by the need to replace the stabilizers at the surface of the particle during the synthesis of the shell. The diffusion in metals is commonly accepted to proceed via migration of atoms into vacancy defects. Correspondingly, the activation barrier for diffusion is the sum of an activation barrier for the creation of the defect and for the migration, $\Delta H = \Delta H_f + \Delta H_m$, respectively. For Au and Ag, $\Delta H = 1.76$ eV, $\Delta H_f = 1.0 \pm 0.15$ eV, and $\Delta H_m = 0.75 \pm 0.10$ eV.[47] Removal of the barrier for creation of the defect at the interface would bring the diffusion coefficient to the level of 10^{-16}–10^{-15} cm^2 s^{-1}, well within the time scale observed for alloying. It should be recognized that in typical bulk metals the density of vacancies is very small, 10^{-3}–10^{-4} per atom, even at the melting point. For most of the particles studied here, this amounts to less than one defect per particle. A single vacancy at the interface is enough to catalyze the fast diffusion rate. Similar explanation is invoked to rationalize high strain and enhanced alloying in the bulk immiscible Ag–Cu combination.[48] The presence of defects at the interface, but not in the interior, will also explain the fast decrease in penetration beyond the first subsurface layer. This will lead to reduced diffusion rate as the atoms penetrate deeper into one another.

It is recognized here that the experimentally observed time scale for Au–Ag alloying (a few days) is much longer than that observed for other bimetallic combinations by Mori and co-workers (seconds to minutes).[10,13] Many reasons may lead to this difference, including lower melting temperatures for one of the components, lattice mismatch between the two metals at the interface (versus a nearly perfect match in the present case), and the presence of the support (versus water and stabilizers in the present work), which may induce additional strain into the lattice and enhance migration of the atoms.

Molecular Dynamics Simulations. Analysis of the molecular dynamics simulations centers on transport properties of atoms within the NPs. Most of the atomic motion is due to surface atoms migrating around the outer spherical shell. Because this motion does not effectively mix the two constituents of the core–shell structure, we have developed a method of estimating the relaxation time for the complete alloying process from our simulations.

The mean square displacement of atoms confined to a spherical volume of radius R approaches $6R^2/5$ in the infinite-time limit. Similarly, the mean square displacement in the *radial* coordinate only (relative to the NP center of mass) approaches $3R^2/40$. At shorter times, one might want to connect the observable displacements of atoms in a simulation to the solutions of the diffusion equation. For a spherically symmetric volume with a reflecting boundary at R, the solutions to the diffusion equation are given by eq 2

$$\rho(r,t) = \sum_{n=1}^{\infty} a_n \frac{\sin(n\pi r/R)}{r} e^{-n^2\pi^2 Dt/R} \tag{2}$$

where the coefficients a_n are determined from the initial concentration profile. Proper mapping of the displacements of the individual atoms onto the diffusion coefficient, D, in this confined geometry would involve projecting the initial and final positions of each atom onto each of the diffusional modes expressed in the summation of eq 2. A simpler approach, and one that is more relevant to the situation at hand, is to compute the relaxation time of the mean square displacement using the known infinite-time limit and the famous Kohlraush–William–Watts (KWW) relaxation law[49,50] that can arise from a sum of exponential decays:

$$\langle |r(t) - r(0)|^2 \rangle \approx \frac{6R^2}{5}(1 - e^{-(t/\tau)^\beta}) \tag{3a}$$

For the alloying process, only displacements in the radial direction lead to mixing. If we use only the radial component of the particle positions to compute the mean square displacements, the prefactor that gives the infinite-time limit must change to $3R^2/40$:

$$\langle |r_{\text{radial}}(t) - r_{\text{radial}}(0)|^2 \rangle \approx \frac{3R^2}{40}(1 - e^{-(t/\tau)^\beta}) \tag{3b}$$

where r_{radial} is the radial coordinate of an atom relative to the NP center. Note that the radial displacements involve different contributions from the diffusional modes in eq 2, so one should expect to observe different values of τ and β in eqs 3a and 3b. Our fits to the mean square radial displacement functions show stretching parameters $\beta \approx 0.8$ in the liquid state, and $\beta \approx 0.4$ below the melting transition. These stretching parameters are merely indicators of multiexponential decay due to the boundary conditions on the diffusion equation. They should not be taken to indicate a system with inhomogeneities similar to those one would see in glasses[51] or defective crystals.[52]

The mixing relaxation times are displayed in a standard Arrhenius plot in Figure 6. At the high end of the temperature scale shown in Figure 6, the particles melt during the calculation (24 or 12 ns). Because diffusion in the melt occurs via a different mechanism from that in the solid, these temperatures were excluded from the linear Arrhenius extrapolation. At temperatures lower than ~500 K, the displacement is too small to provide a reliable estimate of the relaxation times. Even with these limits, the long extrapolation to 300 K provides only an

---

(47) Tu, K.-N.; Mayer, J. W. *Electronic Thin Film Science*; Macmillan: New York, 1992.
(48) Sheng, H.; Ma, E. *Phys. Rev. B* **2001**, *63*, 224205.
(49) Kohlrausch, F. *Ann. Phys. (Berlin)* **1863**, *119*, 352.
(50) Williams, G.; Watts, D. C. *Trans. Faraday Soc.* **1970**, *66*, 80.
(51) Vardeman, C.; Gezelter, D. *J. Phys. Chem. A* **2001**, *105*, 2568.
(52) Rabani, E.; Gezelter, J. D.; Berne, B. J. *Phys. Rev. Lett.* **1999**, *82*, 3649.

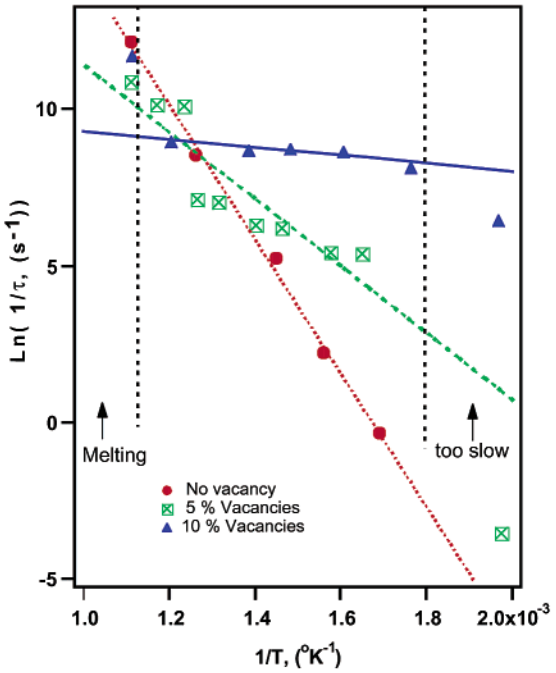

Figure 6. Arrhenius plot of relaxation rates for complete Au−Ag alloying. Triangles, no vacancies; squares, initially 5% vacancies at the interface; circles, 10% vacancies. The two vertical dashed lines indicate the range used for the fits. At temperatures higher than the fitting range, the particles are liquid droplets, and the relaxation times reflect liquid-state transport mechanisms. At temperatures lower than the fitting range, the trajectories were not long enough to provide adequate statistics for the mean squared displacement calculations.

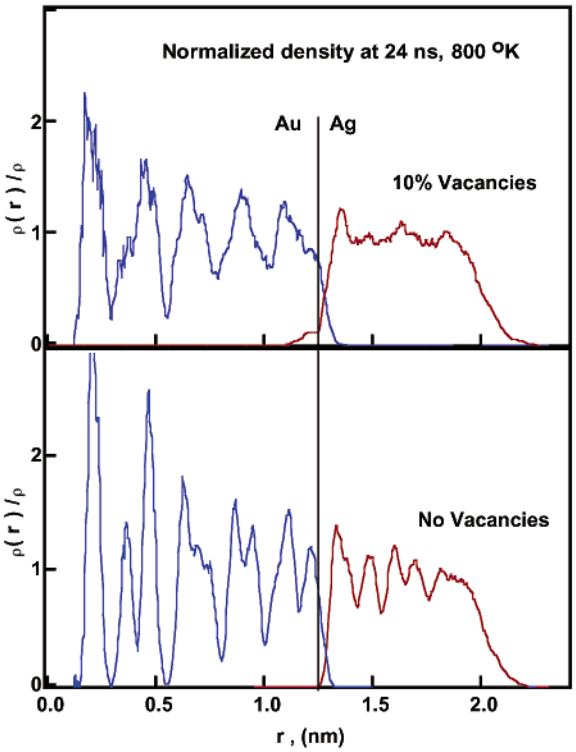

Figure 7. Density profiles of Au and Ag atoms within the NP during the last 2 ns of a 24 ns NVT simulation at 800 K. Bottom profile: no interfacial vacancies. Top profile: 10% initial interfacial vacancies.

order of magnitude estimate of the relaxation time at room temperature. For the core−shell NPs without any vacancies, we obtain from these plots an activation energy of 1.85 eV, similar to experimental determinations,[47] and 0.92 and 0.11 eV for 5% and 10% vacancy levels, respectively. Projecting the Arrhenius plots of the relaxation times down to 300 K, the room-temperature relaxation times are $>10^7$ years at no vacancies, a few days for 5% interfacial vacancies, and minutes to seconds for 10% vacancies. Thus, a few percent of vacancies are probably not far from the present experimental conditions.

Figure 7 shows the radial density profile, $\rho(r)/\rho$, of the two constituents as a function of distance from the center of the NP. This density profile was obtained from the last 2 ns of the 24 ns NVT runs at 800 K. Remarkably, the interfacial vacancies result in a substantial smoothing of the peaks in the density profile, indicating that the particles with interfacial vacancies are closer to the melting transition than those without them. It is evident from the region near $r = 12.5$ Å that the interfacial vacancies result in significantly enhanced radial diffusion of Ag into the core region of the NPs. Most of the displacement, though, occurs along the bimetallic interface (i.e., at constant r), which is clear from the pronounced broadening of the density peaks.

Conclusions

It was shown above that the atoms at the boundary between the two metals in small NPs, which were initially constructed as core−shell structures, spontaneously interdiffuse. The rate of alloying of the two components is size dependent but cannot be explained merely by size-dependent depression of the melting point that leads to enhanced diffusion. We hypothesize that vacancy defects at the boundary between the two metals cause the observed enhancement. Molecular dynamics calculations demonstrate that vacancies at the boundary dramatically enhance the rate of mixing as suggested. To be consistent with the experimental observations, the calculations would require that a few percent of the sites at the bimetallic interface are vacant. That such defects are present, even when the atomic sizes of the two metals are essentially identical, is not a priori expected. Perhaps it is the presence of a stabilizer at the interface during the particle growth that causes these imperfections.

The presence of vacancies at the bimetallic interface can also explain the observed termination of the alloying process. The alloying may be viewed as a competition between percolation of the defects to the outer surface and migration of the metal atoms into the vacancies. Once a vacancy percolates to the outer interface, its penetration back into the lattice is expected to be extremely slow. Preferred directionality in migration toward the surface is expected because of the larger volume fraction and smaller curvature of the outer layers. Furthermore, a higher energy barrier is required to generate a vacancy in the bulk relative to the surface. Both effects will ensure prohibitively slow vacancy penetration back into the bulk. Because the bimetallic interfacial area (per mass unit) is size dependent, a constant vacancy fraction of that area can also explain the size dependence of the mixing process.

The study reported here describes the mixing of two metals of extremely similar dimensions. Also, the bond energies of the Au−Au, Ag−Ag, and Au−Ag couples are relatively similar. A future avenue of investigation is the study of the dependence of the alloying on size and bond energies when these similarities are relaxed. This is currently under investigation in our laboratories.

Acknowledgment. This work is supported by the U.S. Department of Energy (DOE), Office of Science, Basic Energy Sciences. The MRCAT is supported by the DOE under Contract DE-FG02-94-ER45525 and the member institutions. Use of the Advanced Photon Source was supported by the DOE under Contract No. W-31-102-Eng-38. Computational time was provided on the Notre Dame Bunch-of-Boxes (B.o.B.) cluster under NSF grant DMR 00 79647. This is contribution NDRL No. 4287 from the Notre Dame Radiation Laboratory.

JA026764R